

# Material dependent modeling of secondary electron emission coefficients and its effects on PIC/MCC simulation results of capacitive RF plasmas

M Daksha<sup>1,2</sup> , A Derzsi<sup>2,3</sup> , Z Mujahid<sup>4</sup> , D Schulenberg<sup>1</sup>, B Berger<sup>1,5</sup> , Z Donkó<sup>3</sup>  and J Schulze<sup>1,2</sup> 

<sup>1</sup> Institute of Electrical Engineering and Plasma Technology, Ruhr-University Bochum, D-44780 Bochum, Germany

<sup>2</sup> Department of Physics, West Virginia University, Morgantown, WV 26506, United States of America

<sup>3</sup> Institute for Solid State Physics and Optics, Wigner Research Centre for Physics, Hungarian Academy of Sciences, 1121 Budapest, Konkoly-Thege Miklós str. 29–33, Hungary

<sup>4</sup> Department of Physics, Faculty of Science, Jazan University, 45142, Jazan, Saudi Arabia

<sup>5</sup> Electrodynamics and Physical Electronics Group, Brandenburg University of Technology Cottbus-Senftenberg, D-03046 Cottbus, Germany

E-mail: [manudaksha@gmail.com](mailto:manudaksha@gmail.com)

Received 24 September 2018, revised 28 January 2019

Accepted for publication 21 February 2019

Published 25 March 2019



## Abstract

The ion-induced secondary electron emission coefficient ( $\gamma$ ) is a vital parameter in the modeling of low temperature RF plasmas. Often, the value of  $\gamma$  drastically affects the electron power absorption dynamics, the plasma parameters and the quality of the separate control of ion flux and mean ion energy at the electrodes. Experimental results for  $\gamma$  under plasma exposure are difficult to obtain. Therefore,  $\gamma$  is either assumed to be a constant chosen with some uncertainty, or is approximated as a quantity that is a function of the ion energy and cleanliness of the electrode surface. It is hypothesized that these assumptions are not valid for all materials and plasma conditions. In this work, Hagstrum's theory on Auger emission is suggested as a robust, *ab initio* model for accurately predicting  $\gamma$  for metal surfaces with a wide range of surface conditions and for a variety of ion species. To demonstrate the effect of the choice of  $\gamma$  on modeling results, we carry out particle-in-cell/Monte Carlo collision simulations of 13.56 MHz, single-frequency argon and helium capacitive discharges. Simulations are run assuming that: (i)  $\gamma$  is a constant, (ii)  $\gamma$  is an energy and surface condition dependent quantity that is independent of the electrode material, and (iii)  $\gamma$  is obtained from the *ab initio* model for different clean metals. The energy distribution of the emitted electrons resulting from Hagstrum's theory is also implemented as a uniform, metal dependent distribution with physically accurate energy domain. It is found that this is important for some metals in both helium and argon. Lastly, it is observed that, depending on the assumed surface conditions, the plasma properties change dramatically. Based on these results we conclude that a realistic, material dependent implementation of  $\gamma$  is required to obtain realistic simulation results and that Hagstrum's model suits this purpose.

Keywords: capacitive radio frequency plasmas, secondary electron emission coefficients, plasma surface interactions, electron heating, particle in cell simulations, *ab initio* modeling of secondary electron emission coefficients, Auger emission

## 1. Introduction

Radio frequency (RF) discharges are an indispensable tool for surface etching, deposition and sputtering [1–3]. These processes are vital in the production of devices such as solar cells, semiconductors, computational devices, and etc. The desire for high quality, efficiently manufactured devices requires that the plasma interacts with the surface in a controllable manner. Specifically, plasma parameters such as the mean ion energy and ion flux have to be controlled independently. However, in order to obtain such control, it is important to understand how the surface interacts with the plasma and vice versa [4, 5].

Particle-in-cell/Monte Carlo collision (PIC/MCC) simulations serve as an essential tool in studies of RF discharges [6–12]. Despite their detailed kinetic description of the plasma dynamics, PIC/MCC simulations usually have a meager description of surface processes that influence the plasma. For example, only two surface parameters are typically assumed to have any effect on the plasma: the electron reflection probability ( $\rho$ ) and the ion-induced secondary electron emission coefficient ( $\gamma$ ). The assumptions made for these parameters are known to influence the computed discharge properties [4, 13–20]. Important electron ejection phenomena, such as electron-induced secondary electron emission ( $\delta$ ), are still largely ignored. However, powerful models already exist for  $\delta$  and  $\rho$  [21–23]. The implementation of  $\delta$  in PIC/MCC simulations and its effects on the calculated discharge characteristics have already been studied for SiO<sub>2</sub> boundary surfaces [24, 25]. Other electron ejection processes from surfaces by fast neutrals, metastable atoms and VUV photons are also suggested to be important [13, 26]. Bokhan and coauthors have worked on understanding photoemission, and potential, kinetic secondary electron emission under the influence of atom implantation in plasma devices [27–29].

For many applications of capacitively coupled plasmas (CCPs) such as plasma enhanced chemical vapor deposition, and reactive sputtering, the plasma is operated under conditions where the electron heating dynamics are sensitive to the choice of the boundary surface material due to its  $\gamma$ . Specifically, it has been observed that the choice of  $\gamma$  can influence whether the plasma operates in the  $\alpha$ - or  $\gamma$ -power absorption mode for a given pressure and voltage [30]. Furthermore, there have been studies demonstrating the significant effect of  $\gamma$  on the Paschen curve [31], sputtering processes with magnetrons [32], etc  $\gamma$  has also been shown to drastically change sheath characteristics [33, 34].

However, in PIC/MCC simulations of CCPs,  $\gamma$  is either neglected, assumed to be a constant with a typical value of 0.1, or implemented for ‘clean’ and ‘dirty’ metals [26, 35] as a function of incident ion energy but independent of the surface material [13, 18, 36, 37]. Accurate, material specific, description of  $\gamma$  has generally not been sought. This is because relevant experimental data for  $\gamma$  is only available for few metals and incident ion species. These data originate from either beam experiments in ultra high vacuum environment, or from DC plasma breakdown using Paschen’s law. Lastly, in ultra high vacuum beam experiments, the targets are

usually flashed using very high temperatures. Therefore, information about their surface roughness and crystallinity is unknown. Theoretical efforts to calculate  $\gamma$  usually require using a computationally intensive scheme [38, 39]. Since CCPs are utilized for a wide range of surface processing applications, PIC/MCC simulations need access to  $\gamma$  values under a variety of electrode conditions and material type in order to realistically simulate these surfaces. Hence, efficient computation of these  $\gamma$  coefficients is highly desirable.

Hagstrum’s theory on electron emission due to Auger processes [40] is applied here as a simple ab-initio model that can accurately determine  $\gamma$  for any clean metal and ions with low kinetic energies. The effects of the ion kinetic energy on the  $\gamma$  can be predicted by utilizing Hagstrum’s theory in the scope of Auger processes relying on potential emission but this extension of the model and inclusion of kinetic Auger processes is the subject of future research. At very high ion energies of several 100 eV kinetic knockout effects can contribute to secondary electron emission as well. In order to include these effects, which are not related to potential Auger emission, another extension of Hagstrum’s model must be done, which is not the subject of this work either. This restricts the discharge conditions of CCPs our model can be applied to to pressures typically above several 10 Pa, i.e. to the presence of collisional sheaths. In section 2.1, Hagstrum’s model is summarized. The assumptions are outlined and the predictive ability of the theory is demonstrated. Section 2.2 presents the results of this model in terms of selected material dependent  $\gamma$  for different incident ion species. Furthermore, the model results are compared with data from the literature for many atomically clean and contaminated metals under relevant ion energies and species type.

Section 3.1 introduces the PIC/MCC simulation. In order to study the importance of implementing accurate energy distribution functions for the secondary electrons, two different uniform distributions are assumed: (i) the range in energy is between 0 and 5 eV and it is independent of material type, and (ii) the range in energy is given by Hagstrum’s model for the given clean metal. The first assumption is the typical treatment of the secondary electrons in PIC/MCC simulations.

Section 3.2 illustrates PIC/MCC simulation results for single frequency 13.56 MHz discharges in argon, and helium. The simulations are run assuming  $\gamma$  to be a constant 0.1, or by implementing the functional forms for ‘clean’ and ‘dirty’ metals [26, 35] that is dependent on the ion energy but independent on the specific metal type. These are then compared to results obtained by utilizing different  $\gamma$  coefficients obtained for calcium, gold, molybdenum, copper and platinum from Hagstrum’s model. Calcium is simulated to demonstrate discharge characteristics for materials with very high  $\gamma$ . It is known that metals with high  $\gamma$ , such as cesium, are utilized for negative hydrogen ion generation in RF discharges. The plasma density and heating dynamics are demonstrated to be extremely different depending on the model for  $\gamma$  even at relatively low pressures. The implementation of realistic secondary electron energy distributions

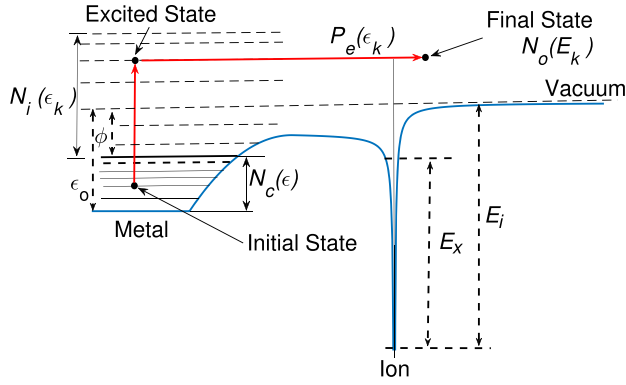


**Figure 1.** A visual summary of the theoretical approach.  $\phi$  is the work function.  $\epsilon_0$  is the metal potential well depth.  $E_i$  and  $E_x$  are the ionization and excitation energies of the ion species, respectively.  $N_c(\epsilon)$  is the initial density of states for electrons in the conduction band.  $N_i(\epsilon_k)$  is the distribution in energy of electrons that have been excited by the process.  $P_e(\epsilon_k)$  is the probability that an excited electron escapes the metal.  $N_o(E_k)$  is the distribution in energy of the escaped electrons.  $\epsilon$  is the initial electron energy.  $\epsilon_k$  and  $E_k$  are the energy of the excited and escaped electrons, respectively.

is found to be important. Finally, conclusions are drawn in section 4.

## 2. Calculation of ion-induced secondary electron emission coefficients ( $\gamma$ )

### 2.1. Hagstrum's model

In the following section, we summarize a model originally developed by Hagstrum [40] to calculate ion-induced secondary electron emission coefficients ( $\gamma$ ) based on potential Auger processes. These processes are dominant at low ion energies where radiative processes have a very long lifetime and there is not enough kinetic energy for kinetic emission to take place. As the theory is not widely known, a more extended summary is provided here.

Hagstrum's model is based on Fermi's golden rule. Therefore, only adiabatic processes are considered. This makes energy conservation arguments an integral part of implementing different ejection processes. To begin, the specific excitation mechanisms that lead to electron emission must be specified. The model holds two processes responsible for the excitation of electrons inside the metal (section 2 of [40]):

- (i) the Auger neutralization of an ion (figure 2)
- (ii) the resonance neutralization (figure 3) of an ion followed by Auger de-excitation (figure 4) of the metastable.

Before delving further into the details of the processes, the theoretical approach responsible for electron ejection is summarized as in figure 1.

The ejection process can be thought of in the following way: there is an initial electron configuration described by the

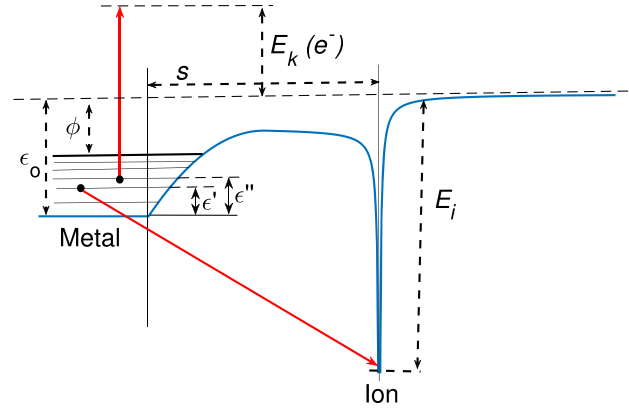


**Figure 2.** Auger neutralization: the red lines represent transition to the final state.  $E_k(e^-)$  is the kinetic energy of the escaped electron,  $s$  is the distance between ion and metal surface,  $\phi$  is the work function,  $E_i$  is the ionization energy of the ion,  $\epsilon_0$  is the well depth,  $\epsilon'$ , and  $\epsilon''$  are the initial energies of the electrons undergoing Auger neutralization.

density of states in the metal conduction band ( $N_c(\epsilon)$ ). When the ion approaches the metal, at a certain distance  $s$ , excitation occurs where either of the two processes mentioned above takes place. The excited electrons (they still have not escaped the metal) have a distribution in energy described by  $N_i(\epsilon_k)$ . Finally, the probability of the electron escaping ( $P_e(\epsilon_k)$ ) depends on the direction of its velocity vector relative to the surface normal. The entire process results in a distribution of escaped electrons ( $N_o(E_k)$ ) that can be integrated over all energies to obtain  $\gamma$ .

It should be noted that the two processes can occur without there being any ejection. This can be important when considering dielectric materials where the energy band gap is high and the conduction band is empty. The material properties (i.e. conductivity) can still be influenced by these processes because electrons are excited into the dielectric conduction band.

**2.1.1. Auger neutralization.** The mechanism of Auger neutralization is illustrated in figure 2. Two electrons are initially in the metal potential well with some energy,  $\epsilon'$ , and  $\epsilon''$  (section 3 of [40]). As the ion approaches the surface at distance  $s$ , neutralization takes place and one of the electrons neutralizes the ion. The electron rests in the ground state of the atom. The resulting change in energy is transferred to another electron in the metal, effectively ejecting it. The resulting energy conservation argument can be written as follows:

$$\epsilon_k = \epsilon' + \epsilon'' - \epsilon_0 + E_i. \quad (1)$$

In equation (1), the energy of the excited electron is  $\epsilon_k$ . It is assumed that there are no energy level shifts due to the interaction of the ion and metal. Also, the total energy of the system is assumed to be zero. As can be seen,  $\epsilon_k$  depends on the initial energy of the electrons ( $\epsilon'$ ,  $\epsilon''$ ). In order to determine the distribution of excited electrons in the metal, it

is important to take into account every possible combination of starting energies the electrons can have before the process. This is a difficult combinatorial problem that can be reduced by assuming that:  $\epsilon' = \epsilon + \Delta$  and  $\epsilon'' = \epsilon - \Delta$ . This then gives the Auger Transform (section 3 of [40]):

$$T(\epsilon) = \begin{cases} \int_0^\epsilon N_c(\epsilon - \Delta)N_c(\epsilon + \Delta)d\Delta & , \text{ if } 0 < \epsilon < \frac{\epsilon_F}{2} \\ \int_0^{\epsilon_F - \epsilon} N_c(\epsilon - \Delta)N_c(\epsilon + \Delta)d\Delta & , \text{ if } \frac{\epsilon_F}{2} < \epsilon < \epsilon_F \\ 0 & , \text{ if } \epsilon < 0, \epsilon > \epsilon_F \end{cases} \quad (2)$$

It should be noted that the Auger Transform is obtained for a Fermi distribution at absolute zero. Any attempt to apply a Fermi distribution for higher temperatures without changing the transform will lead to a lowering of the  $\gamma$ . This is because the limits of integration are 0, and the Fermi energy,  $\epsilon_F$ . As the temperature increases, the probability of finding an electron in this region lowers. However, if the ionization level is high enough to eject electrons with low initial electron energies, then the  $\gamma$  due to Auger neutralization will be constant as a function of temperature. This is because only states close to  $\epsilon_F$  are affected by a change in temperature. So, the only observable difference would be a high energy tail in  $N_o(E_k)$ .

Arifov has experimentally measured the dependence of  $\gamma$  on the temperature [41]. This was done for helium and argon ions impinging on tantalum, molybdenum, tungsten, nickel, zircon, and platinum. He observed that  $\gamma$  is constant if the surface is atomically clean. This is in excellent agreement with the above analysis.

Equation (2) gives the distribution of electrons over a given central energy,  $\epsilon$ . In order to determine the distribution of excited electrons ( $N_i(\epsilon_k)$ ), one has to simply shift this distribution over energy using equation (1) and take into account the states that are available for the excited electrons ( $N(\epsilon_k)$ ). This leads to:

$$N_i(\epsilon_k) = \begin{cases} \frac{N(\epsilon_k)T[\frac{\epsilon_k + \epsilon_o - E_i}{2}]}{\int_{\epsilon_F}^{\infty} N(\epsilon_k)T[\frac{\epsilon_k + \epsilon_o - E_i}{2}]d\epsilon_k} & , \text{ if } \epsilon_k > \epsilon_F \\ 0 & , \text{ if } \epsilon_k < \epsilon_F \end{cases} \quad (3)$$

**2.1.2. Auger de-excitation.** Unlike Auger neutralization, Auger de-excitation is a two step process (section 4 of [40]). First, resonance neutralization of the ion must take place (figure 3). This is followed by Auger de-excitation (figure 4). The process can be described as follows: an electron from the metal tunnels into a degenerate state(s) shared between the ion and metal. This neutralizes the ion and creates an excited atom or metastable. Now that resonance neutralization has happened, there are two pathways for Auger de-excitation to take place. The first possibility is that an electron from the metal transitions to the ground state of

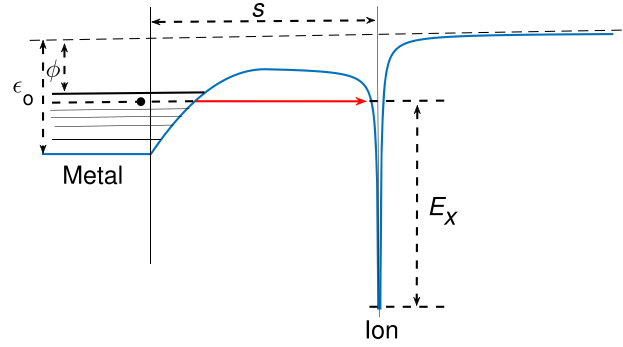


**Figure 3.** Resonance neutralization: the dashed black lines represent the degenerate energy level shared between ion and metal.  $E_x$  is the excitation energy,  $\phi$  is the work function,  $\epsilon_o$  is the well depth, and  $s$  is the distance between ion and metal surface.

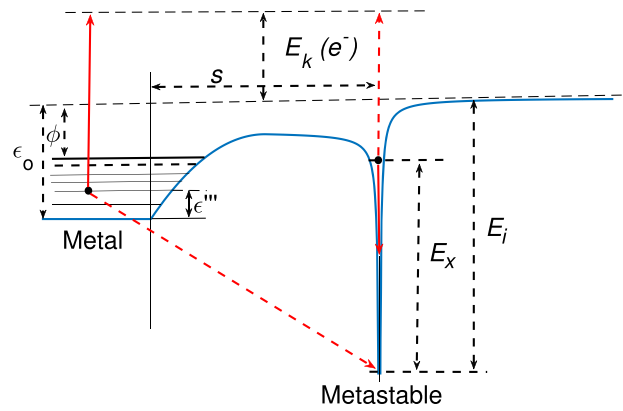


**Figure 4.** Auger de-excitation: the dashed lines express de-excitation through electron exchange. The solid lines represent de-excitation through non-exchange.  $\epsilon'''$  is the initial energy of the electrons,  $\phi$  is the work function,  $\epsilon_o$  is the metal potential well depth,  $E_i$  and  $E_x$  are the ionization and excitation energies of the ion species, respectively.  $E_k(e^-)$  is the kinetic energy of the escaped electron, and  $s$  is the distance between the ion and the metal surface.

the metastable. This then causes the electron at the excited energy level to escape. This is called the electron exchange pathway. The second possibility is that the excited electron de-excites to the ground state. This allows an electron in the metal to escape. This is called non-exchange pathway. Focusing specifically on the non-exchange pathway, the energy conservation argument can be written as:

$$\epsilon_k = \epsilon''' + E_x, \quad (4)$$

where  $E_x$  is the first excitation energy level of the ion and  $\epsilon'''$  is the initial energy of the electron in the conduction band. There is no implementation of energy level shifts due to the interaction of the metastable or ion with the metal. The energy conservation argument is much simpler because only the fact that there exists an electron at an excited state needs to be taken into account. Therefore, only one electron in the metal has a variable energy. This leads to a much simpler Auger

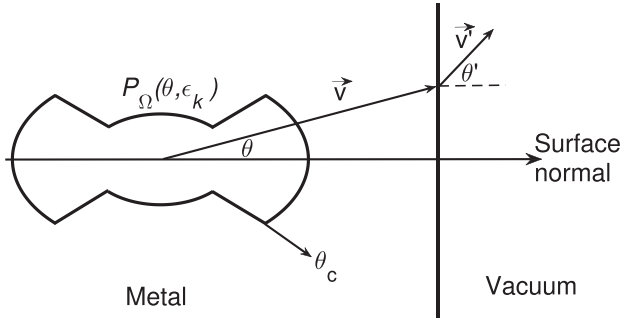


**Figure 5.** A visual representation of how to obtain  $P_e(\epsilon_k)$ . First, an anisotropic distribution is assumed for  $P_\Omega(\theta, \epsilon_k)$ . When an electron leaves the metal, it has to lose energy equal to the metal potential well ( $\epsilon_o$ ). This results in refraction. The critical angle ( $\theta_c$ ) is the largest angle at which the electron can escape the metal ( $\theta' = \frac{\pi}{2}$  when  $\theta = \theta_c$ ).

Transform for Auger de-excitation (section 4 of [40]):

$$T'(\epsilon) = N_c(\epsilon). \quad (5)$$

Lastly, the same ideology can be applied to obtain the distribution of electrons excited by Auger de-excitation as was used for Auger Neutralization:

$$N_i'(\epsilon_k) = \begin{cases} \frac{N(\epsilon_k)T[\epsilon_k - E_x]}{\int_{\epsilon_F}^{\infty} N(\epsilon_k)T[\epsilon_k - E_x]d\epsilon_k} & , \text{ if } \epsilon_k > \epsilon_F \\ 0 & , \text{ if } \epsilon_k < \epsilon_F \end{cases}. \quad (6)$$

**2.1.3. Calculation of  $\gamma$ .** Two major assumptions are made in order to determine the distribution of excited electrons for both process. First, it is assumed that the probability of either Auger neutralization or Auger de-excitation to occur is unity. Second, the probability of these processes to occur on the inward trip to the metal (before collision with the surface) is assumed to be unity as well. Section 5 of Hagstrum's paper, briefly attempts to justify these assumptions [40].

Referring back to figure 1, it can be seen that the model has been built up to the point that the rest of the process can be discussed without involving a specific excitation pathway. The next step is to obtain an analytical form for the probability that an excited electron is ejected ( $P_e(\epsilon_k)$ ). This is done by first assuming a probability that the velocity vector of an excited electron is pointing at a direction relative to the surface normal with a certain energy ( $P_\Omega(\theta, \epsilon_k)$ ). An anisotropic distribution is assumed for this probability, as seen in figure 5.

In order to escape the metal, the escaping electron needs to have enough energy parallel to the surface normal. After the electron escapes, it loses that amount of energy and this causes refraction. Therefore, a critical angle can be calculated due to this refraction. Once this is done,  $P_\Omega(\theta, \epsilon_k)$  is made artificially anisotropic by introducing a fitting parameter,  $f$ . Throughout this paper,  $f$  is assumed to be a constant 2.

Hagstrum used a value of 2.2 for  $f$  by roughly fitting it to experimental results for helium on tungsten. However, the difference in the resulting  $P_e(\epsilon_k)$  is negligible.  $P_e(\epsilon_k)$  is obtained by integrating  $P_\Omega(\theta, \epsilon_k)$  over all possible angles with which the excited electron can escape (section 6 of [40]):

$$P_e(\epsilon_k) = \begin{cases} \frac{1}{2} \frac{1 - \left(\frac{\epsilon_o}{\epsilon_k}\right)^{\frac{1}{2}}}{1 - \left(1 - \frac{1}{f^2} \left(\frac{\epsilon_o}{\epsilon_k}\right)^{\frac{1}{2}}\right)} & , \text{ if } \epsilon_k > \epsilon_o \\ 0 & , \text{ if } \epsilon_k < \epsilon_o \end{cases}. \quad (7)$$

The distribution of escaped electrons is then simply obtained by taking a product of the distribution of excited electrons and the probability of them escaping:

$$N_o(\epsilon_k) = N_i(\epsilon_k)P_e(\epsilon_k). \quad (8)$$

$\gamma$  is then the integral of  $N_o$  over all energies:

$$\gamma = \int_0^{\infty} N_o(E_k)dE_k. \quad (9)$$

Now that the model has been developed such that electron yields can be obtained for both Auger neutralization and de-excitation, it is important to recognize the fact that these processes are mutually exclusive. Furthermore, the model predicts Auger neutralization to happen much farther away from the surface than Auger de-excitation. This is explained by the fact that resonance neutralization is a tunneling process and requires the ion to be close to the metal. This means that Auger neutralization must be the dominant process.  $\gamma_{\text{Neut}}$  is the probability of electron ejection when Auger neutralization takes place. Similarly,  $\gamma_{\text{De-exc}}$  is the probability of electron ejection when Auger de-excitation takes place. Therefore, the following is assumed about the contribution of each process (sections 11 and 14 of [40]):

$$\gamma_T = 0.9\gamma_{\text{Neut}} + 0.1\gamma_{\text{De-exc}}, \quad (10)$$

where  $\gamma_T$  is the total secondary electron emission coefficient. The coefficients in equation (10) have been determined by Hagstrum. This has been justified by comparing the range in energy of the distribution of the escaped electrons ( $N_o(\epsilon_k)$ ) between experiment and model. Most of the experimental distributions have a range in energy that associates with the energy minimum and maximum that is defined by Auger neutralization.

Lastly, as can be seen from the derivation of the model, there are several potentially significant effects that have not been taken into account, such as shifts in energy levels, finite lifetimes, broadening of energy levels due to Heisenberg's uncertainty principle, and etc. Despite Hagstrum's attempts to implement these effects (sections 8, 9, 10 and 12 of [40]), there are many inaccuracies and disagreements between experiments and model results. The accurate implementation of these effects is the subject of further research.

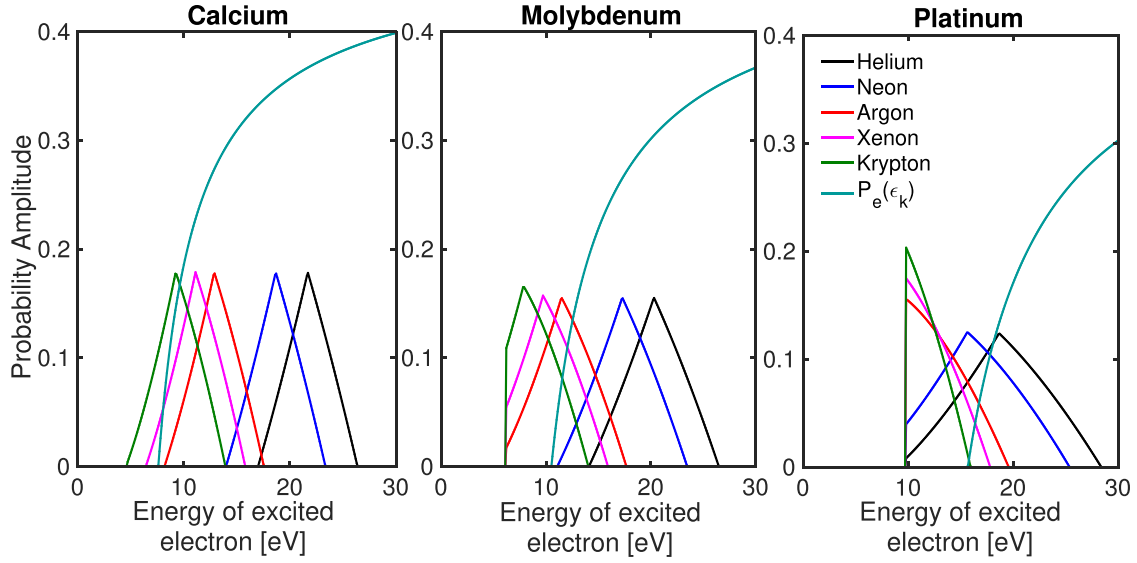


**Figure 6.** Normalized distribution of excited electrons ( $N_e(\epsilon_k)$ ) and the probability that an electron escapes the metal as a function of the energy of excited electron for calcium, molybdenum and platinum for different incident ion species.

## 2.2. Calculation of $\gamma$ for various metals and surface properties

It is important to discuss the distribution of excited electrons in the surface and of escaped electrons obtained from Hagstrum's model. Since Auger neutralization is assumed to be the dominant process, only distributions relating to this process are shown for calcium, molybdenum and platinum for different noble gas ions.

Figure 6 shows that the higher the ionization energy of the incident ion, the greater the shift in the distribution of excited electrons; the electrons can be excited to a higher energy state. The work function of the surface plays a role in determining the probability of escape of the excited electrons. As can be seen in the case of molybdenum and platinum, the distributions for argon, krypton and xenon cut off at the low energy domain. This is because any electron that has an energy less than the Fermi energy is not considered to be excited.

Lastly, the width of the distribution is largely dependent on the Fermi energy. A higher Fermi energy implies that there are more occupied states, and therefore, the number of excited states that can be occupied increases. The width of the distribution is closely related to the amplitude as well because the distributions are normalized. Therefore, a wider distribution of excited electrons will result in a lower probability of finding them at one particular energy.

There is an exception to this observation which occurs when the well depth is greater than the ionization energy for some electrons. This results in a lower allowed energy domain, and thus, an increase in amplitude. This is seen for the case of platinum where krypton has the highest peak and this peak decays as the ionization energy of the noble gas increases.

The distribution of escaped electrons shown in figure 7, for different surface materials and incident ion species, can be

compared to experimental results [40–42]. This model does not accurately describe the general shape of the functions that are obtained experimentally, because it does not take energy broadening effects such as surface image charges into account. However, it gives accurate information on where the maxima occur and the general width of the distributions in energy.

It is hypothesized that, the distribution of escaped electrons must be realistically implemented in simulations of low temperature plasmas. For example, given that a helium ion is impinging on the metal, molybdenum can emit an electron with a maximum energy of 18.7 eV and is most likely to produce an electron with 14.11 eV. Platinum can emit an electron with a maximum energy of 12.6 eV and is most likely to emit an electron with just 5.13 eV. This is an additional material dependence that can significantly influence the plasma. It is hypothesized that, at high pressures, the starting energies of the electrons will matter: the position at which, within the sheath, the first ionization happens relative to the electrode will significantly affect the electron's ability to ionize and multiply in the sheath. An electron with a higher initial energy can ionize closer to the electrode and start the Townsend multiplication sooner. These maximum and minimum energies of escaped electrons can be calculated by taking energy arguments from figure 2 and are given by equations (11) and (12). It is important to note that  $E = 0$  eV is not the vacuum level but the lowest energy occupied state in the metal conduction band

$$E_{\min} = \begin{cases} E_i - 2\epsilon_o & , \text{if } E_i > 3\epsilon_o \\ 0 & , \text{else} \end{cases} \quad (11)$$

$$E_{\max} = 2\epsilon_F + E_i - 2\epsilon_o. \quad (12)$$

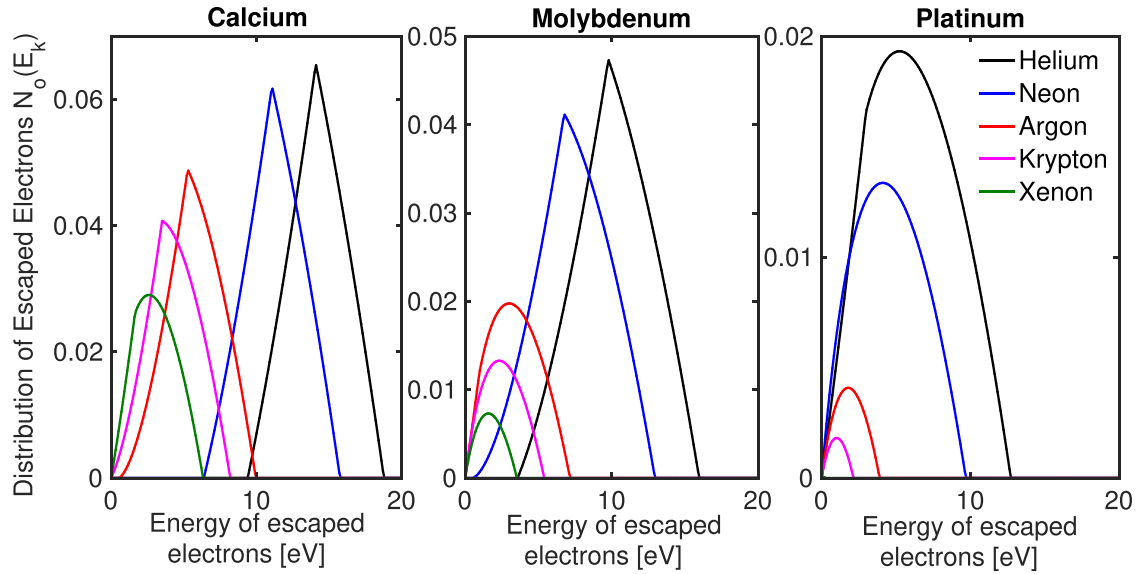


**Figure 7.** Distribution in energy of the escaped electrons ( $N_0(E_k)$ ) as a function of escaped electron energy for different surface materials and incident ion species.

Table 1 compares  $\gamma$  obtained by Hagstrum's model to that obtained experimentally for different metals. Although comprehensive, this is by no means a complete list of experimental data for metals under these conditions. Most of the values for the work function are either given in the paper where  $\gamma$  is experimentally determined or obtained from Derry [43]. For the Fermi energy, all the values are either obtained through Ashcroft [44], or they are calculated by assuming a spherical Fermi surface and obtaining free electron densities from the NIST database [45]. Exceptions to this rule have their Fermi energy and work function taken from Oechsner [46]. It should be noted that the fitting parameter  $f$  in equation (7) was held at a constant 2.

Generally, a good agreement is found between the experimental data and results from the model calculations. The discrepancy in the experimental results obtained for molybdenum were studied by Vance [48]. The disagreements are a consequence of the cleaning mechanism (flashing) being inadequate to remove carbon from the target. Vance also found that heating with the presence of  $O_2$  produces results in agreement with Hagstrum's yield for molybdenum and produces an atomically clean surface. This explains many experimental values where the  $\gamma$  seems to be significantly lower than the expected value. However, it is unknown in these experiments whether the carbon is adsorbed onto the surface or exists in the bulk of the target. Furthermore, there are significant problems in atomically cleaning a metal surface by heating. It is known that heating increases the porosity of the metal and allows it to adsorb impurities. This is the reason for the huge difference in experimental results for tantalum and zircon. Lastly, if the substrate is heated close to its melting point under discharge operation, then nanotendrils or 'fuzz' can develop on the surface. Indeed, it has been observed by Patino that such structures can change (lower in this case) the  $\gamma$  [62].

It should be noticed that the anisotropy in the work function can depend on the substrate thickness [63]. Furthermore, Eastment has also shown that sputter cleaning aluminum can cause a reordering of the surface structure [63]. The reordering can drastically change the work function, and therefore the  $\gamma$ . There is an observed coupling between the thickness of aluminum and the surface orientation on the work function. These effects have a significant influence on  $\gamma$  that can be predicted using Hagstrum's model via the implementation of the changed work function.

There are significant disagreements between model and experimental results obtained by Arifov [41]. However, it should be noted that the results for tantalum, and nickel in table 1, obtained by Arifov, are quite different than what is obtained by Takeishi and Molnar, respectively [47, 59]. From the authors' understanding of Arifov's methodology, it seems as though Arifov grew the films on a substrate and the film thickness is about 40nm. Under this regime, the crystal orientation should significantly affect the work function as in [63], and therefore, the  $\gamma$ . Furthermore, some substrate parameters might be influenced by the material that it was grown on.

The effect of surface roughness on  $\gamma$  is not known. However, there exist models and experimental results for the influence of surface roughness on the work function as obtained by Li [64]. These can be implemented into the model to determine their influence on the discharge in a PIC/MCC simulation.

Most CCP discharges contain electrodes that are not atomically clean. Therefore, it is important to understand the effects of adsorption of different particle species on the work function. Furthermore, the  $\gamma$  can be accurately calculated for metals with impurities as seen in table 1, provided that the effect of these impurities on the work function and Fermi energy are known [48, 49]. However, if there are significant

**Table 1.** Comparison of  $\gamma$  obtained from Hagstrum's model with literature data for different surface material and incident ion species.

Surface material	Ion	Experimental $\gamma$	Hagstrum's model
Nb	Ar <sup>+</sup>	0.137 [46]	0.115
Pd	Ar <sup>+</sup>	0.077 [46]	0.064
Cu	Ar <sup>+</sup>	0.082 [46]	0.078
Ti	Ar <sup>+</sup>	0.148 [46]	0.119
Ag	Ar <sup>+</sup>	0.088 [46]	0.077
Ni (111)	He <sup>+</sup>	0.170 [47]	0.177
Ni (111)	Ne <sup>+</sup>	0.128 [47]	0.111
Ni (111)	Ar <sup>+</sup>	0.034 [47]	0.030
C contaminated Mo	He <sup>+</sup>	0.247 [48]	0.275 ± 0.005
C contaminated Mo	Ar <sup>+</sup>	0.066 [48]	0.077 ± 0.008
He contaminated Ta	He <sup>+</sup>	0.14 [49]	0.13
Al	Ar <sup>+</sup>	0.05 [50], 0.08 [51]	0.08
K	Ne <sup>+</sup>	0.38 ± 0.01 [41]	0.23 ± 0.01
K	Ar <sup>+</sup>	0.26 ± 0.01 [41]	0.21 ± 0.01
Na	Ne <sup>+</sup>	0.36 ± 0.01 [41]	0.27 ± 0.01
Na	Ar <sup>+</sup>	0.25 ± 0.01 [41]	0.24 ± 0.01
Ba	Ne <sup>+</sup>	0.34 ± 0.01 [41]	0.28 ± 0.01
Ba	Ar <sup>+</sup>	0.24 ± 0.01 [41]	0.24 ± 0.01
Zr	Ne <sup>+</sup>	0.14 [41]	0.22
Zr	Ar <sup>+</sup>	0.04 [41]	0.08
Zr	Ar <sup>+</sup>	0.14 [46]	0.14
Ni	Ne <sup>+</sup>	0.19 ± 0.01 [41]	0.190
Ni	Ar <sup>+</sup>	0.07 ± 0.01 [41], 0.078 [46]	0.051
Au	He <sup>+</sup>	0.16 [52], 0.18 ± 0.02 [53]	0.26
Au	Ne <sup>+</sup>	0.15 ± 0.02 [53]	0.21
Au	Ar <sup>+</sup>	0.062 [46], 0.02 [52], 0.07 ± 0.01 [53]	0.06
Mo	He <sup>+</sup>	0.286 [48], 0.300 [54], 0.20 [55]	0.287
Mo	Ne <sup>+</sup>	0.254 [54], 0.228 [56]	0.247
Mo	Ar <sup>+</sup>	0.127 [48], 0.122 [54], 0.083 [55], 0.074 [56], 0.035-0.051 [57, 58], 0.071 [59], 0.08 [60]	0.101
Mo	Kr <sup>+</sup>	0.069 [54], 0.053 [55]	0.055
Mo	Xe <sup>+</sup>	0.022 [54]	0.022
Ta	Ne <sup>+</sup>	0.23 ± 0.01 [41]	0.11 ± 0.01
Ta	Ar <sup>+</sup>	0.026 [59], 0.013 [61]	0.029
Ta	Ar <sup>+</sup>	0.11 ± 0.01 [41], 0.117 [46]	0.08
Pt	Ne <sup>+</sup>	0.07 ± 0.01 [41]	0.08
Pt	Ar <sup>+</sup>	0.03 ± 0.01 [41], 0.021 [61]	0.02 ± 0.01

impurities in the bulk material, then the  $\gamma$  can be influenced without a significant change in work function [48].

It is observed that most experimentalists only obtain  $\gamma$  for one or two gases. Hagstrum's model successfully alleviates this problem. As long as the condition of the electrode is known under a given gas, it can be utilized to determine the  $\gamma$  for a different inert gas species.

It should be noted that the notion of a 'dirty' metal surface as prescribed by Phelps and Petrović is rather general [26]. It is important to know the composition of material that is adsorbed on the surface as different gases can affect the  $\gamma$  in different and very significant ways [32, 61].

Finally, there have been many computational studies on the influence of  $\gamma$  on CCPs [4, 65–68]. However, the authors usually vary the  $\gamma$  in a step like fashion. They show the discharge's sensitivity to  $\gamma$  without prescribing the  $\gamma$  to a particular electrode type and electrode condition. Now, it is

possible to put into context exactly what range of  $\gamma$  is possible for a CCP with a certain electrode configuration.

### 3. Effect of $\gamma$ on PIC/MCC simulation results of CCPs

#### 3.1. PIC/MCC method

A 1d3v, electrostatic particle-in-cell simulation with Monte Carlo treatment of collisions (PIC/MCC) is utilized to simulate a geometrically symmetric CCP [12, 13, 69]. The approach has been shown to be capable of predicting realistic kinetic effects in CCPs [70–73]. The geometry is planar with infinite parallel electrodes that are set apart by 2.5 cm. The gases utilized are helium and argon. The background gas temperature is held at a constant 350 K. The probability of an electron reflecting from the surface is kept at 0.2 independent of surface conditions [74]. It is assumed that both

**Table 2.** Predicted minimum and maximum energy for escaped electrons in Helium.

Material	$E_{\min}$	$E_{\max}$
Mo	3.38 eV	15.8 eV
Au	0.00 eV	13.6 eV
Pt	0.00 eV	13.6 eV

**Table 3.** Predicted minimum and maximum energy for escaped electrons in Argon.

Material	$E_{\min}$	$E_{\max}$
Ca	0.58 eV	9.96 eV
Mo	0.00 eV	7.16 eV
Cu	0.00 eV	6.76 eV
Pt	0.00 eV	4.76 eV

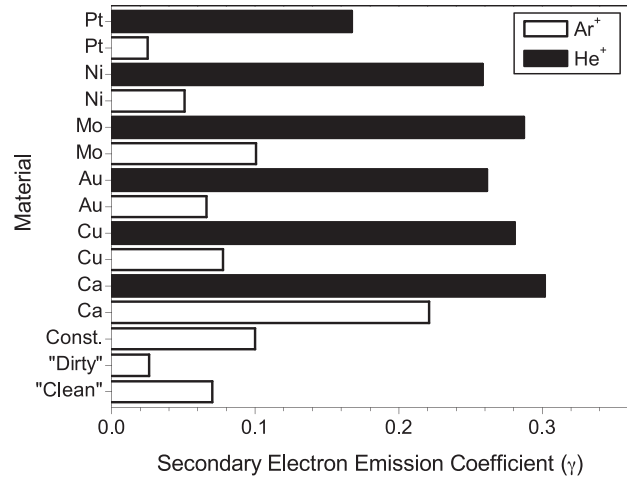
electrodes are made of the same material with identical surface conditions.

For  $\gamma$ , two different assumptions are compared with the Hagstrum model results for argon. The first assumption sets  $\gamma$  to 0.1 irrespective of the material and conditions. The second assumption determines an effective  $\gamma$  depending on the energy distribution of the impinging ion, according to [26, 35]. Only the effect of choosing different metals for electrodes according to Hagstrum's model will be shown for simulated helium CCPs. The electron-neutral and ion-neutral collision cross sections are taken from [75–77] and [78] for argon and helium, respectively.

Simulations are performed for a single frequency discharge with the driving voltage waveform:  $V(t) = V_0 \cos(2\pi ft)$  with  $f = 13.56$  MHz. The powered electrode is at  $x = 0$  cm. The other electrode is grounded. The voltage amplitude for both gases is fixed to 300 V. The pressure is varied for argon from 10 to 130 Pa. For helium, the pressure is varied from 90 to 270 Pa. The metals considered for argon are molybdenum, copper, calcium and platinum. For helium, they are molybdenum, gold and platinum.

In PIC/MCC simulations, the emitted electrons have to be seeded with a certain initial energy. A general recipe on assigning the angle and initial energy has been given by Surendra and Graves [79]. In this paper, uniform energy distributions for escaped electrons are implemented in two different ways: (i) the energies are assumed to be between a minimum and maximum energy from Hagstrum's model given in section 2.2., or (ii) the energies are assumed to be between 0 and 5eV independent of the type of metal. The first approach is typical for PIC/MCC simulations. In this way, the importance of implementing realistic  $N_o(\epsilon_k)$  in PIC/MCC simulations is studied. The energy ranges are shown in tables 2 and 3.

The implemented distributions are set as uniform because the model does not provide accurate information on the shape of  $N_o(\epsilon_k)$ . However, it does give accurate information on the relevant domain of the distribution function. Therefore, we


**Figure 8.** Comparison of  $\gamma$  for different surface materials and helium and argon ions, respectively, based on Hagstrum's model. Constant  $\gamma = 0.1$  and  $\gamma$  obtained from an analytical description proposed in [26] for 'clean' and 'dirty' metals are shown for comparison. There was virtually no energy dependence for 'clean' and 'dirty' metals under the specified discharge conditions.

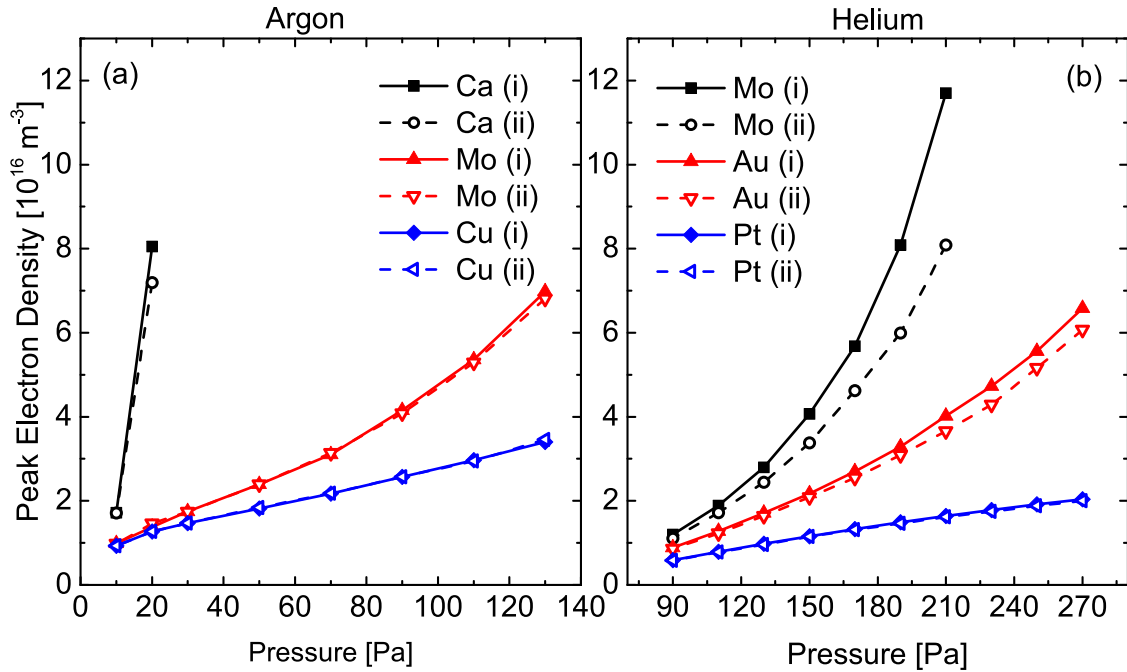
determine the sensitivity of plasma properties to the metal specific energy domain of the emitted electrons.

For  $\gamma$  not obtained by Hagstrum's model, a uniform distribution is assumed with electron energies between 0 and 5 eV.

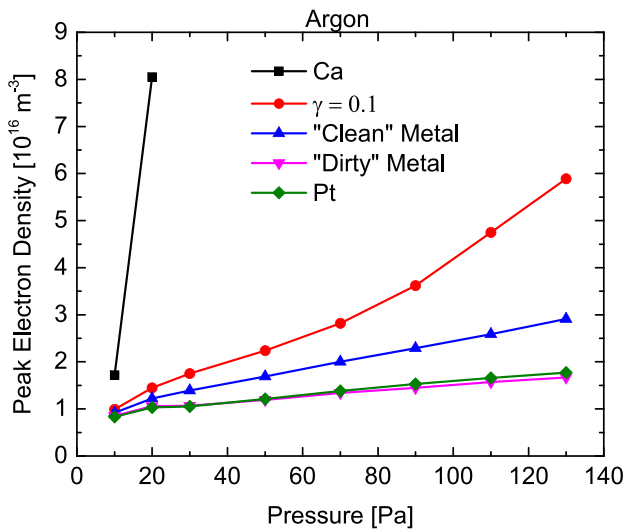
### 3.2. Results

Figure 8 is a visual comparison of  $\gamma$  for helium and argon obtained by using Hagstrum's model for different surface materials.  $\gamma$  obtained based on an analytical expression proposed by Phelps and Petrovic [26] for 'clean' and 'dirty' metals is shown as well. The requisite input for the incident ion energies is provided by the PIC/MCC simulations under the conditions described in section 3.1 for argon. Finally, the case of  $\gamma = 0.1$  is also shown in figure 8. While the  $\gamma$  obtained for helium is higher on average, the range in  $\gamma$  for the metals is much greater for argon than helium. A lot of metals reach a similar value of  $\gamma$  in helium of approximately 0.3. This is because the ionization energy is so high that all electrons within the metal conduction band can be excited and emitted with a non zero probability. Therefore, the difference in the metals is mostly a matter of the shape and range of the distribution of escaped electrons ( $N_o(E_k)$ ). Since the mean ion energies are low and energy dependence is not significant under this regime, it might be of interest to implement constant  $\gamma$  coefficients for different adsorbed gases predicted by Hagstrum's model.

It is important to ascertain whether the energy distributions obtained from Hagstrum's model are important to implement. This is checked in our simulations, for which the results are displayed in figure 9. In these simulations, material specific  $\gamma$  obtained from Hagstrum's model is utilized alongside different implementations of the energy distributions of emitted electrons.



**Figure 9.** PIC/MCC simulation results for the peak electron densities for (a) argon and (b) helium plasmas as a function of pressure, obtained using material specific  $\gamma$  given by Hagstrum’s model. The energies of the escaped electrons are between: (i) a minimum and maximum energy from Hagstrum’s model, or (ii) 0 and 5 eV independent of the type of metal. Discharge conditions: 13.56 MHz, 300 V, 2.5 cm.



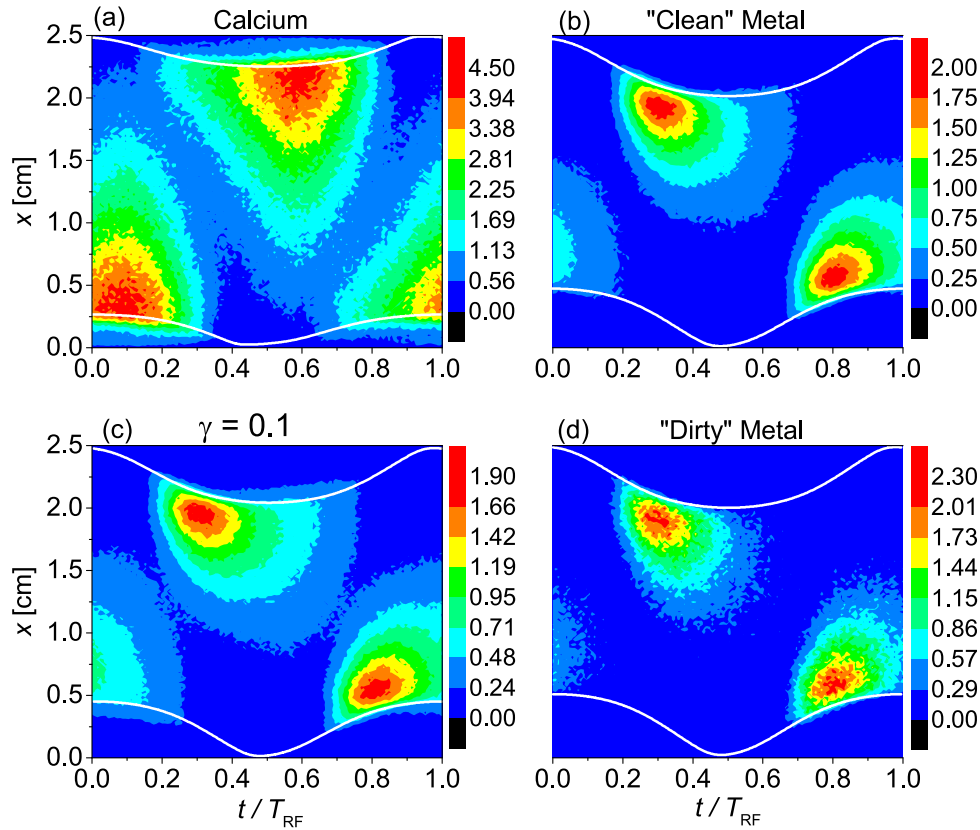
**Figure 10.** Peak electron density as a function of pressure for an argon CCPs obtained from PIC/MCC simulations based on  $\gamma$  obtained from Hagstrum’s model for calcium and platinum surfaces, based on an analytical expression provided by Phelps and Petrovic for ‘dirty’ and ‘clean’ metals [26], and based on  $\gamma = 0.1$ . The results are for a single frequency, 13.56 MHz discharge with a voltage amplitude of 300 V for Ar and a gap length of 2.5 cm. For Ca and Pt, the value of  $\gamma$  and the energy domain for the emitted electrons is given by Hagstrum’s model. The other results are obtained based on the assumption that all emitted electrons are equally likely to be emitted in the domain of 0 and 5 eV.

Results are obtained based on assuming: (i) a minimum and maximum energy from Hagstrum’s model, or (ii) 0 and 5 eV independent of the type of metal. For argon, we find a good agreement between results for the different schemes for most

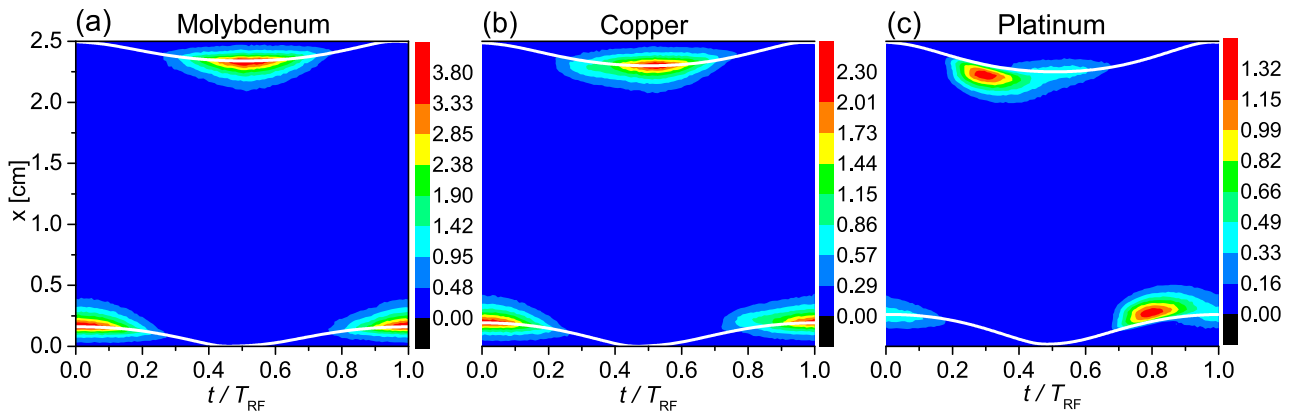
metals. However for calcium, there is a 14% difference in the peak electron density for the specific discharge conditions considered. This is believed to be due to a synergistic effect between a high  $\gamma$  and the probability that electrons with higher energies can escape the metal. For helium, a significant difference is found in the plasma density for molybdenum electrodes, while for other metals the two schemes give very similar values. As most industry relevant metals have work functions and Fermi energies close to molybdenum, implementation of realistic escaped electron distributions is important for CCP simulations in helium.

Figure 10 shows unequivocally that classical assumptions employed for describing ‘clean’ metals, such as utilizing  $\gamma = 0.1$  for all metals, are simply insufficient. It is true that, under certain conditions here, the ‘clean’ and ‘dirty’ and  $\gamma = 0.1$  simulations resemble densities that can be obtained by a specific metal. However, in general, they cannot individually explain the range of densities that can be obtained.

It is known that alkali metals, such as cesium, are often utilized for negative hydrogen ion generation in RF discharges [80]. Arifov has demonstrated that even a few monolayers of alkali metals can significantly affect the  $\gamma$  [41]. However, the agreement between the model and experimental results for potassium and sodium were quite different. Alkali earth metals like magnesium had experimental  $\gamma$  that agreed well with the model. Furthermore, the alkali earth metals have only slightly lower  $\gamma$  when compared to alkali metals. Therefore, calcium seemed to be a good choice in order to demonstrate the diversity in discharge conditions that could be potentially obtained in an RF discharge. These results can



**Figure 11.** Spatiotemporal plots of the electron-impact ionization rate obtained from PIC/MCC simulations of a CCP operated in argon at 20 Pa (13.56 MHz, 300V) using  $\gamma$ : (a) for calcium from Hagstrum's model, (b) for 'clean' metals [26], (c) for  $\gamma = 0.1$ , and (d) for dirty metals [26]. The white lines signify the sheath width at each electrode as a function of time. The color scales are in units of  $10^{20} \text{ m}^{-3} \text{ s}^{-1}$ . All simulations presented in this figure assume that the emitted electrons are equally likely to be ejected in the energy domain of 0 and 5 eV.



**Figure 12.** Spatiotemporal plots of the electron-impact ionization rate obtained from PIC/MCC simulations of a CCP operated in argon at 130 Pa (13.56 MHz, 300 V) using  $\gamma$  obtained from Hagstrum's model: (a) for molybdenum, (b) for copper, and (c) for platinum. The white lines signify the sheath width at each electrode as a function of time. The color scales are in units of  $10^{21} \text{ m}^{-3} \text{ s}^{-1}$ . All metals have their energy domains for emitted electrons described by Hagstrum's model.

also be experimentally validated by using methods such as  $\gamma$ -CAST [81].

Figure 11 shows the spatiotemporal distribution of the ionization rate obtained from the simulations for the different assumptions about the electrode. As can be seen, in a CCP operated at 13.56 MHz, 20 Pa and with  $V_0 = 300 \text{ V}$ , for calcium electrodes, the discharge operates in  $\gamma$ -mode while the

other simulations, which implement classical assumptions for  $\gamma$ , operate in  $\alpha$ -mode. This is because  $\gamma$  is high enough for calcium such that efficient multiplication of secondary electrons can take place in the sheath to increase the plasma density. This lowers the sheath width. The sheath edge is marked by white lines in the figures and determined according to the criteria given by Brinkmann [82]. The simulation with

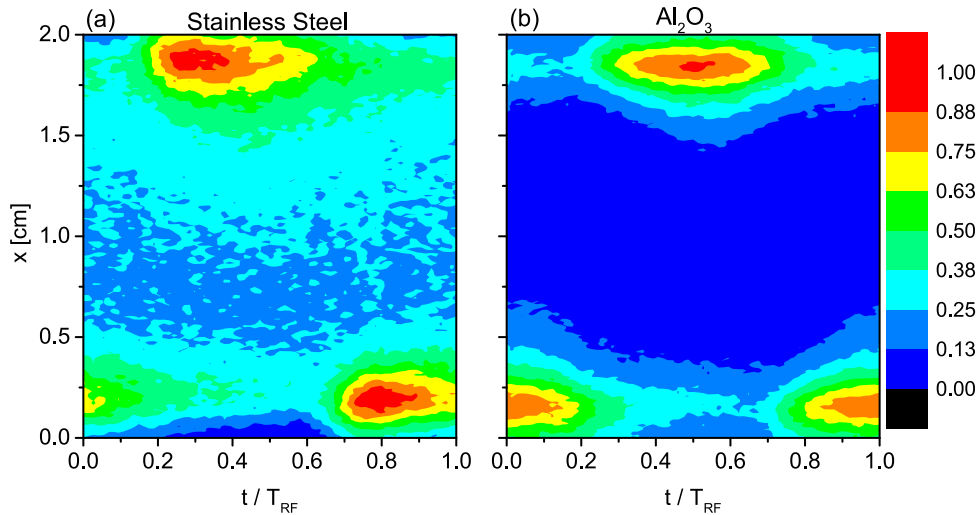


**Figure 13.** Spatiotemporal plots of the electron-impact excitation rates obtained from PROES measurements of a symmetric CCP operated in argon with 10% neon admixture at 125 Pa (13.56 MHz, 140 V) using: (a) stainless steel electrodes, (b) aluminum oxide electrodes. The figures were normalized to their respective maxima.

$\gamma$  of 0.1 shows signs of transitioning into  $\gamma$ -mode power absorption. The simulations for ‘clean’ and ‘dirty’ metals predict strong  $\alpha$ -mode power absorption at this pressure.

Figure 12 shows that at high pressures, the difference in the power absorption dynamics are further enhanced. As can be seen from figure 12, for molybdenum and copper electrodes the discharge operates in pure  $\gamma$ -mode, while for platinum the discharge remains in  $\alpha$ -mode. The  $\gamma$ -mode power absorption is much more localized at these high pressures. This is in sharp contrast to the  $\gamma$  mode achieved by Calcium at a much lower pressure of 20 Pa.

#### 4. Conclusions

In this paper, Hagstrum’s model [40] was applied as a useful *ab initio* tool for obtaining accurate, metal dependent secondary electron emission coefficients ( $\gamma$ ). The derivation of the model has been outlined to explicitly state some of the pivotal assumptions and their influence on the calculated  $\gamma$  to be utilized in PIC/MCC simulations. Furthermore, the basic theory was utilized to show no temperature dependence of  $\gamma$  for ‘clean’ metals.

Experimentally determined  $\gamma$  from different authors, under low ion energies and for inert gases and various different metals were compared with Hagstrum’s model. A good agreement was found between experimental results and model results. Any differences can be explained by a specific surface property and its effect on the work function. It is known that effects like surface adsorption, chemisorption, surface roughness, corrosion, among others can significantly influence the work function [41, 63, 64]. Therefore, by implementing the relevant work function, the effect of a specific surface condition can be predicted using PIC simulations in conjunction with the suggested model. Diagnostics such as  $\gamma$ -CAST can potentially compare experimental and simulation

results [81]. This methodology can determine whether  $\gamma$  obtained using ultra high vacuum beam experiments can truly be utilized in predicting plasma behavior. However, the exploration of these topics is the subject of a future work.

The energy distributions of escaped electrons for different metals have been shown for different gas species to discuss whether including them in PIC/MCC simulations is necessary for better emulation of a realistic surface. The importance of incorporating these distributions was examined. Uniform distributions were implemented that either had an energy domain that was independent of the metal type and between 0 and 5 eV, or had an energy maxima and minima determined by Hagstrum’s model.

PIC/MCC simulations were ran for single frequency argon and helium capacitive RF discharges. Specifically, for argon, calcium, molybdenum, copper and platinum electrodes were simulated based on realistic, material specific  $\gamma$  obtained from Hagstrum’s model. First, the effect of different assumptions for the energy distributions of the escaped electrons on the plasma were compared. It was found that, for argon, the assumption of a metal independent distribution seemed to be satisfactory for non alkali, alkali earth metals. However, this assumption was not sufficient for helium. Then, the simulation results for these metals were compared with the common assumptions that either  $\gamma$  is a constant 0.1 or that it can be described as a function of the incident ion energy that is generalized for ‘clean’ and ‘dirty’ metals [26, 35]. Classical assumptions were found to be insufficient to capture the true range of observed plasma density that can be obtained when simulating the specific metals realistically. It was also found that the electron power absorption dynamics are strongly dependent on the type of metal. Therefore, ‘classical’ assumptions are insufficient in predicting plasma phenomena for the entire range of ‘clean’ metals. For helium, the discharge was simulated with molybdenum, gold and platinum electrodes. There was a significant difference in the

behavior of the plasma depending on the material. This was represented by the difference in the peak electron density as a function of pressure.

Recently, phased resolved optical emission spectroscopy (PROES) measurements were taken with a symmetric cell similar to the one utilized in  $\gamma$ -CAST [81]. Figure 13 provides results for such a setup where a symmetric CCP is operated with a frequency of 13.56 MHz, a driving voltage amplitude of 140 V, and a pressure of 125 Pa in argon with 10% neon admixture as a tracer gas for PROES. There is a massive difference in the heating dynamics when comparing metal electrodes to those made of stoichiometric  $\text{Al}_2\text{O}_3$ . This difference becomes apparent by comparing the time within the RF period, when a maximum of the excitation rate is observed adjacent to a given electrode. For instance, at the top electrode and in case of stainless steel electrodes a maximum of the excitation rate is observed during the phase of sheath expansion at  $t/T_{\text{RF}} \approx 0.3$ , while for  $\text{Al}_2\text{O}_3$  electrodes the corresponding maximum is found at the time of maximum sheath expansion at the top electrode of  $t/T_{\text{RF}} \approx 0.5$ . These experimental findings agree qualitatively with the computational results shown in figure 12, where the ionization rate at the top electrode was found to be maximum during sheath expansion at  $t/T_{\text{RF}} \approx 0.3$  for platinum electrodes figure 12(c), while a maximum is observed at the time of maximum local sheath expansion of  $t/T_{\text{RF}} \approx 0.5$  for molybdenum and copper electrodes (figures 12(a) and (b)). The CCP with electrodes made of aluminum oxide is operated in the  $\gamma$  electron heating mode, while the CCP operated with stainless steel electrodes under otherwise identical conditions remains in the  $\alpha$  electron heating mode. This suggests that the  $\gamma$  for aluminum oxide under these conditions is higher than the  $\gamma$  for stainless steel. Important effects such as surface charging, color defects, negative ion generation at the surface, impact of fast neutrals, and photon emission can contribute to the higher  $\gamma$ . The identification of the relevant effects and their implementation into the pre-existing model is the subject of a future work. Nevertheless, these experimental findings verify the importance of using realistic material dependent SEECs as input parameters for plasma models/simulations.

## Acknowledgments

This work was supported by the US NSF grant no. PHY1601080, by the German Research Foundation (DFG) within the frame of the collaborative research centers SFB-TR 87 project C1, and SFB 1316 (project A4), and by the Hungarian National Research, Development and Innovation Office (NRDI Office) via grants K-119357 and PD-121033. The authors would like to thank FX Bronold for the useful discussions. A Derzsi thanks the support from the J Bolyai Scholarship of the Hungarian Academy of Sciences. M Daksha thanks the Daksha family for their unfaltering support.

## ORCID iDs

M Daksha  <https://orcid.org/0000-0002-5190-8401>  
 A Derzsi  <https://orcid.org/0000-0002-8005-5348>  
 Z Mujahid  <https://orcid.org/0000-0002-3661-8596>  
 B Berger  <https://orcid.org/0000-0001-7053-2545>  
 Z Donkó  <https://orcid.org/0000-0003-1369-6150>  
 J Schulze  <https://orcid.org/0000-0001-7929-5734>

## References

- [1] Lieberman M A and Lichtenberg A J 2005 *Principles of Plasma Discharges and Materials Processing* 2nd edn (NJ: Wiley)
- [2] Makabe T and Petrović Z 2006 *Plasma Electronics: Applications in Microelectronic Device Fabrication* (London: Taylor and Francis)
- [3] Chabert P and Braithwaite N 2011 *Physics of Radio-Frequency Plasmas* (Cambridge: Cambridge University Press)
- [4] Schulze J, Donkó Z, Schüngel E and Czarnetzki U 2011 *Plasma Sources Sci. Technol.* **20** 045007
- [5] Bronold F X, Fehske H, Pamperin M and Thiessen E 2018 *Eur. Phys. J. D.* **72** 88
- [6] Birdsall C K and Langdon A B 1985 *Plasma Physics via Computer Simulation* (New York: McGraw-Hill)
- [7] Hockney R W and Eastwood J W 1981 *Computer Simulation Using Particles* (New York: McGraw-Hill)
- [8] Birdsall C K 1991 *IEEE Trans. Plasma Sci.* **19** 65
- [9] Diomede P, Capitelli M and Longo S 2005 *Plasma Sources Sci. Technol.* **14** 459
- [10] Matyash K, Schneider R, Taccogna F, Hatazarna A, Longo S, Capitelli M, Tskhakaya D and Bronold F X 2007 *Contrib. Plasma Phys.* **47** 595
- [11] Verboncoeur J P 2005 *Plasma Phys. Contrib. Fusion* **47** A231
- [12] Donkó Z 2011 *Plasma Sources Sci. Technol.* **20** 24001
- [13] Derzsi A, Korolov I, Schüngel E, Donkó Z and Schulze J 2015 *Plasma Sources Sci. Technol.* **24** 034002
- [14] Korolov I, Derzsi A, Donkó Z, Schüngel E and Schulze J 2016 *Plasma Sources Sci. Technol.* **25** 015024
- [15] Bojarov A, Radmilović-Radjenović M and Petrović Z L J 2010 *Proc. 20th ESCAMPIG (Novi Sad, Serbia, 13–17 July 2010)*  
 Bojarov A, Radmilović-Radjenović M and Petrović Z L J 2010 *Publ. Astron. Obs. Belgr.* **89** 131  
 Bojarov A, Radmilović-Radjenović M and Petrović Z L J 2012 *Proc. 65th Annual Gaseous Electronics Conf. (Austin, Texas, 22–26 October 2012)*  
 Bojarov A, Radmilović-Radjenović M and Petrović Z L J 2014 *Proc. 27th Summer School and Int. Symp. on the Physics of Ionized Gases (Belgrade, Serbia, 26–29 August 2014)*
- [16] Radmilović-Radjenović M and Petrović Z L J 2009 *Eur. Phys. J. D* **54** 445
- [17] Gudmundsson J T, Kawamura E and Lieberman M A 2013 *Plasma Sources Sci. Technol.* **22** 035011
- [18] Hannesdóttir H and Gudmundsson J T 2016 *Plasma Sources Sci. Technol.* **25** 055002
- [19] Greb A, Niemi K, O'Connell D and Gans T 2013 *Appl. Phys. Lett.* **103** 244101
- [20] Daksha M, Derzsi A, Wilczek S, Trieschmann J, Mussenbrock T, Awakowicz P, Donkó Z and Schulze J 2017 *Plasma Sources Sci. Technol.* **26** 085006
- [21] Vaughan J R M 1989 *IEEE Trans. Electron Devices* **36** 1963–67
- [22] Bronold F X and Fehske H 2015 *Phys. Rev. Lett.* **115** 225001
- [23] Bronold F X and Fehske H 2017 *Plasma Phys. Control. Fusion* **59** 014011

- [24] Horváth B, Daksha M, Korolov I, Derzsi A and Schulze J 2017 *Plasma Sources Sci. Technol.* **26** 124001
- [25] Horváth B, Schulze J, Donkó Z and Derzsi A 2018 *J. Phys. D: Appl. Phys.* **51** 355204
- [26] Phelps A V and Petrović Z L J 1999 *Plasma Sources Sci. Technol.* **8** R21–44
- [27] Bokhan A P, Bokhan P A and Zakrevsky D E 2005 *Appl. Phys. Lett.* **86** 151503
- [28] Bokhan P A and Zakrevsky D E 2007 *Tech. Phys.* **52** 104
- [29] Bokhan P A and Zakrevsky D E 2013 *Phys. Rev. E* **88** 013105
- [30] Belenguer P and Boeuf J P 1989 *Phys. Rev. A* **41** 4447
- [31] Adams S F, Demidov V I, Kudryavstev A A, Kurlyandskaya I P, Miles J A and Tolson B A 2017 *J. Phys.: Conf. Ser.* **927** 012001
- [32] Depla D, Mahieu S and De Gryse R 2009 *Thin Solid Films* **517** 2825–39
- [33] Campanell M D, Khrabrov A V and Kaganovich I D 2012 *Phys. Rev. Lett.* **108** 255001
- [34] Campanell M D and Umansky M V 2016 *Phys. Rev. Lett.* **116** 085003
- [35] Phelps A V, Pitchford L C, Pédoussat C and Donkó Z 1999 *Plasma Sources Sci. Technol.* **8** B1–2
- [36] Braginsky O, Kovalev A, Lopaev D, Proshina O, Rakhimova T, Vasilieva A, Voloshin D and Zyryanov S 2012 *J. Phys. D* **45** 015201
- [37] Bogaerts A and Gijbels R 2002 *Plasma Sources Sci. Technol.* **11** 27
- [38] Pamperin M, Bronold F X and Fehske H 2017 *Plasma Sources Sci. Technol.* **27** 084003
- [39] Valdés D, Goldberg E C, Blanco J M and Monreal R C 2005 *Phys. Rev. B* **71** 245417
- [40] Hagstrum H D 1954 *Phys. Rev.* **96** 336–65
- [41] Arifov U A 1969 *Interactions of Atomic Particles with a Solid Surface* 1st edn (New York: Springer Science and Business)
- [42] Corbella C, Marcak A, de los Arcos T and von Keudell A 2016 *J. Phys. D: Appl. Phys.* **49** 16T01
- [43] Derry G N, Kern E M and Worth E H 2015 *J. Vac. Sci. Technol. A* **33** 060801
- [44] Ashcroft N W and Mermin N D 1976 *Solid State Physics* (Philadelphia, PA: Saunders)
- [45] Berger M J, Coursey J S, Zucker M A and Chang J NIST Standard Reference Database 124 <https://doi.org/10.18434/T4NC7P>
- [46] Oechsner H 1976 *Phys. Rev. B* **17** 3
- [47] Takeishi Y and Hagstrum H D 1964 *Phys. Rev.* **137** 2A
- [48] Vance D W 1967 *Phys. Rev.* **164** 2
- [49] Hagstrum H D 1953 *Phys. Rev.* **91** 3
- [50] Marcak A, Corbella C, de los Arcos T and von Keudell A 2015 *Rev. Sci. Instrum.* **86** 106102
- [51] Yamauchi Y and Shimizu R 1983 *Japan. J. Appl. Phys.* **22** L227
- [52] Töglhofer K, Aumayr F and Winter H P 1992 *Surf. Sci.* **281** 143–52
- [53] Lakits G, Arnau A and Winter H 1990 *Phys. Rev. B* **42** 1
- [54] Hagstrum H D 1956 *Phys. Rev.* **104** 3
- [55] Varney R N 1954 *Phys. Rev.* **93** 1156
- [56] Mahadevan P, Layton J K and Medved D B 1963 *Phys. Rev.* **129** 79
- [57] Lauer E J 1952 *J. Appl. Phys.* **23** 300
- [58] Theobald J K 1953 *J. Appl. Phys.* **24** 123
- [59] Molnar J P 1951 *Phys. Rev.* **83** 940
- [60] Medved D B, Mahadevan P and Layton J K 1963 *Phys. Rev.* **129** 2086
- [61] Parker J H Jr 1954 *Phys. Rev.* **93** 1148
- [62] Patino M, Raites Y and Wirz R 2016 *Appl. Phys. Lett.* **109** 201602
- [63] Eastment R M and Mee C H B 1973 *J. Phys. F: Met. Phys.* **3** 9
- [64] Li W and Li D Y 2005 *J. Chem. Phys.* **122** 064708
- [65] Sun A, Becker M M and Loffhagen D 2018 *Plasma Sources Sci. Technol.* **27** 054002
- [66] Zhao L, Yue Liu and Samir T 2018 *Chin. Phys. B* **27** 025201
- [67] Hemke T, Trieschmann J, Wollny A, Brinkmann R P and Mussenbrock T 2011 arXiv:1105.4509 [physics.plasm-ph]
- [68] Donkó Z, Schulze J, Hartmann P, Korolov I, Czarnetzki U and Schüngel E 2010 *Appl. Phys. Lett.* **97** 081501
- [69] Donkó Z, Schulze J, Czarnetzki U, Derzsi A, Hartmann P, Korolov I and Schüngel E 2012 *Plasma Phys. Control. Fusion* **54** 124003
- [70] Taccogna F and Dilecce G 2016 *Eur. Phys. J. D* **70** 251
- [71] Rauf S and Kushner M J 1999 *IEEE Trans. Plasma Sci.* **27** 1329
- [72] Lee J K, Babaeva N, Kim H C, Manuilenko O and Shon J W 2004 *IEEE Trans. Plasma Sci.* **32** 47
- [73] Lee H-C and Chung C-W 2012 *Appl. Phys. Lett.* **101** 244104
- [74] Kollath R 1956 *Encyclopedia of Physics* ed S Flüge vol 21 (Berlin: Springer) p 264
- [75] Phelps A V [http://jilawww.colorado.edu/~avp/collision\\_data/](http://jilawww.colorado.edu/~avp/collision_data/) unpublished
- [76] Phelps A V 1991 *J. Phys. Chem. Ref. Data* **20** 557
- [77] Phelps A V 1994 *J. Appl. Phys.* **76** 747
- [78] Biagi S 2004 (Magboltz version 7.1), [www.lxcat.net](http://www.lxcat.net)
- [79] Surendra M and Graves D B 1992 *IEEE Trans. Plasma Sci.* **19** 144
- [80] Guster R, Fantz U and Wunderlich D 2010 *Rev. Sci. Instrum.* **81** 02A706
- [81] Daksha M, Berger B, Schuengel E, Korolov I, Derzsi A, Koepke M, Donkó Z and Schulze J 2016 *J. Phys. D: Appl. Phys.* **49** 234001
- [82] Brinkmann R P 2007 *J. Appl. Phys.* **102** 093303